LETTER

Corrected: Author Correction

https://doi.org/10.1038/s41586-018-0778-7

Direct observation of incommensurate magnetism in Hubbard chains

Guillaume Salomon[1]*, Joannis Koepsell[1], Jayadev Vijayan[1], Timon A. Hilker[1], Jacopo Nespolo[2,3], Lode Pollet[2], Immanuel Bloch[1,2] & Christian Gross[1]

The interplay between magnetism and doping is at the origin of exotic strongly correlated electronic phases and can lead to novel forms of magnetic ordering. One example is the emergence of incommensurate spin-density waves, which have wavevectors that do not belong to the reciprocal lattice. In one dimension this effect is a hallmark of Luttinger liquid theory, which also describes the low-energy physics of the Hubbard model[1]. Here we use a quantum simulator that uses ultracold fermions in an optical lattice[2–8] to directly observe such incommensurate spin correlations in doped and spin-imbalanced Hubbard chains using fully spin- and density-resolved quantum gas microscopy. Doping is found to induce a linear change in the spin-density wavevector, in excellent agreement with predictions from Luttinger theory. For non-zero polarization we observe a reduction in the wavevector with magnetization, as expected from the antiferromagnetic Heisenberg model in a magnetic field. We trace the microscopic-scale origin of these incommensurate correlations to holes, doublons (double occupancies) and excess spins, which act as delocalized domain walls for the antiferromagnetic order. In addition, by inducing interchain coupling we observe fundamentally different spin correlations around doublons and suppression of incommensurate magnetism at finite (low) temperature in the two-dimensional regime[9]. Our results demonstrate how access to the full counting statistics of all local degrees of freedom can be used to study fundamental phenomena in strongly correlated many-body physics.

One-dimensional (1D) quantum systems are paradigmatic examples of the breakdown of Landau Fermi-liquid theory. The free quasiparticles that are present in higher dimensions are replaced by collective excitations, leading to striking phenomena such as spin–charge separation[1]. Luttinger liquid theory[10] generically describes the low-energy physics of gapless 1D systems ranging from quasi-1D conductors and spin liquids to chiral edge modes in the fractional quantum Hall effect[11]. In particular, the repulsive single-band Hubbard model, which provides a minimal microscopic-scale description of doped antiferromagnets, can be described through this approach. Away from half-filling, Luttinger liquid theory predicts incommensurate magnetism with an algebraically decaying incommensurate spin-density wave (SDW) at zero temperature, whose vector varies linearly with density[1]. Also, the presence of a spin imbalance in the 1D Hubbard model can lead to incommensurate spin correlations[12]. Short-range incommensurate magnetism is expected to survive at finite temperature, where conformal field theory predicts an exponential decay of the spin correlations with distance[13]. Luttinger liquids have been experimentally studied in traditional condensed matter systems such as carbon nanotubes via conductance and scanning tunnelling microscopy measurements[14,15]. In particular, magnetism on weakly coupled quasi-1D spin-1/2 chains[16,17] and on ladder systems[18] has been studied using neutron scattering. In higher dimensions, incommensurate SDWs have been detected in underdoped regions of certain high-temperature superconductors via neutron scattering[19]. An interpretation of the results in terms of holes organized in stripes has been proposed, which results in an effective 1D description of the higher-dimensional systems in which the stripes form domain walls in the antiferromagnet. Here we use real-space spin- and density-resolved quantum gas microscopy to directly study the effects of both doping and polarization on finite-range spin correlations in the 1D Hubbard model. We measure the linear change in the SDW vector as a function of density, in excellent agreement with quantum Monte Carlo (QMC) calculations. In the presence of a spin population imbalance, we observe an increase of the SDW wavelength with polarization, as predicted by Luttinger liquid theory and in good agreement with exact diagonalization calculations of the Heisenberg chain. Finally, we report on the evolution of antiferromagnetic spin correlations around doublons in the crossover from one to two dimensions. We find the magnetic environment around doublons to change fundamentally when spin correlations appear in the transverse direction, suggesting the formation of a magnetic polaron[9].

Our experiments started by loading a balanced two-dimensional (2D) degenerate spin mixture of ^{6}Li atoms in the two lowest Zeeman

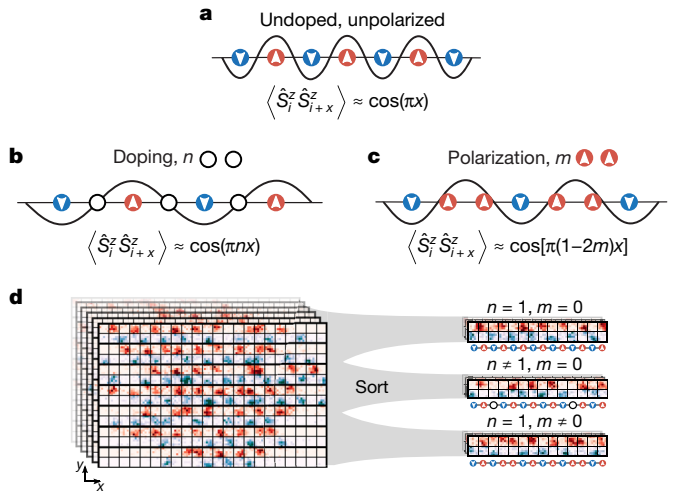

Fig. 1 | Probing incommensurate spin correlations in Hubbard chains. **a**, Spin correlations in spin-balanced Hubbard chains at half filling ($n = 1$) form at a commensurate wavevector π. Red (blue) circles with white up (down) arrows denote up (down) spins. **b**, When the system is doped ($n \neq 1$), incommensurate spin correlations at wavevector πn develop owing to delocalized holes and doublons, which increase the distance between antiferromagnetically correlated spins. **c**, At finite polarization $m \neq 0$, incommensurate spin correlations at a wavevector $\pi(1 - 2m)$ arise owing to excess spins. **d**, Left, single-spin and density-resolved experimental images, each containing seven independent Hubbard chains along y, separated by thick lines, where up (down) spins are represented in red (blue). Right, in post-analysis, we group the data by polarization and doping to analyse their individual effect on spin correlations along x.

[1]Max-Planck-Institut für Quantenoptik, Garching, Germany. [2]Fakultät für Physik, Ludwig-Maximilians-Universität, Munich, Germany. [3]INO-CNR BEC Center and Dipartimento di Fisica, Universita di Trento, Povo, Italy. *e-mail: guillaume.salomon@mpq.mpg.de

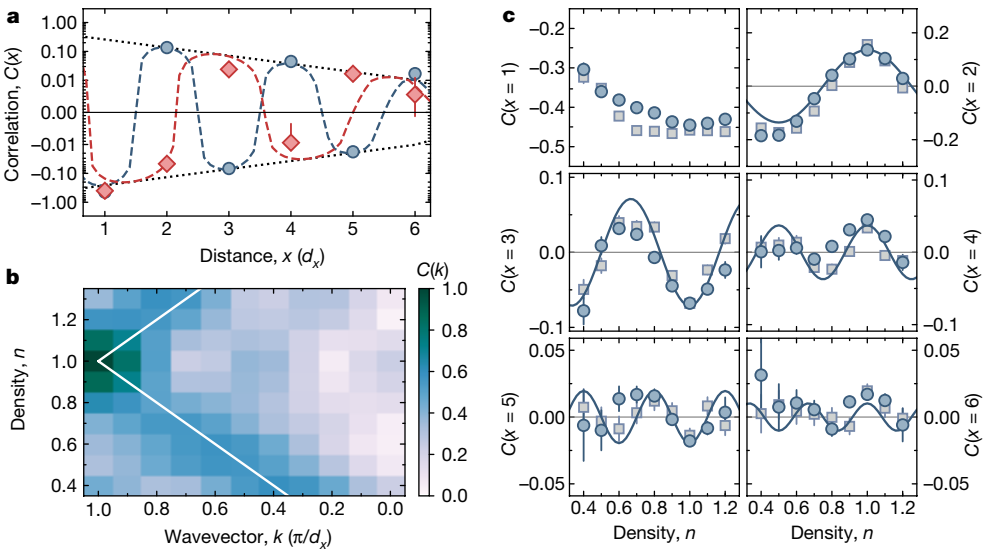

Fig. 2 | Incommensurate spin correlations versus doping. a, Spin correlations $C(x)$ at half-filling (blue) and at $n = 0.7$ (red). The dotted lines show the decay obtained from an exponential fit of the rectified spin correlations $(-1)^x C(x)$ at half-filling. The dashed lines are the Luttinger liquid theory predictions, calculated using the amplitude and decay length obtained from a fit of the $n = 1$ experimental data. The sign change observed for $d \geq 2$ in the doped case originates from delocalized holes stretching the distance between antiferromagnetically correlated spins. **b**, Away from half-filling, the normalized Fourier transform of the spin correlations $C(k)$ reveals a linear increase of the SDW wavevector with density. The white line is the Luttinger liquid theory result $k_{\mathrm{SDW}} = \pi n$. **c**, Spin correlations $C(x)$ versus density at fixed distances $x = 1, \ldots, 6$ (blue dots) compared to QMC calculations at $T = 0.29t_x$ (grey squares). The measured densities are binned in intervals of 0.1. The blue lines are the Luttinger liquid theory prediction with wavevectors πn, calculated using the amplitude and decay length extracted from the fit in **a**. Error bars in all panels denote one standard error of the mean.

states, $|\uparrow\rangle$ and $|\downarrow\rangle$, into an optical lattice formed by two standing waves with period $d_x = 1.15\ \mu\mathrm{m}$ in the x direction and $d_y = 2.3\ \mu\mathrm{m}$ in the y direction (Fig. 1)[5]. The atoms were trapped in a single plane of a vertical lattice with 3.1 μm spacing and a depth of $17E_{\mathrm{r}}^{z}$ where E_{r}^{i} denotes the recoil energy in direction i. The nearest-neighbour tunnelling rates were set to $t_x/h = 410$ Hz at a lattice depth of $5E_{\mathrm{r}}^{x}$ and $t_y/h = 1.2$ Hz at $27E_{\mathrm{r}}^{y}$ to study the 1D Hubbard model (h is the Planck constant). By decreasing the lattice depth in the y direction and ramping up the x lattice power to vary t_y/t_x, we can explore the Hubbard model through the dimensional crossover from one to two dimensions. The on-site interaction U was controlled using the broad Feshbach resonance located at 834.1 G and set to $U = 7t_x$ in the 1D regime. We directly measured the occupation and spin on each lattice site by first freezing the atomic motion before a local Stern–Gerlach-like splitting of the spin components in a superlattice along y (see ref. [5] and Fig. 1). Finally we detected the atoms via Raman sideband cooling[20]. Thanks to the ultimate resolution of our detection technique, which can detect single atoms and spins, we are able to group our data according to the total spin $S^z = (N_\uparrow - N_\downarrow)/2$ and total atom number $N = N_\uparrow + N_\downarrow$, that is, the sum of the numbers of atoms with up and down spins in each chain. These conserved quantities fluctuate for different chains and experimental runs (see Extended Data Fig. 1); however, data grouping allows us to explore the effect of doping and spin imbalance individually (see Fig. 1).

We first study the evolution of antiferromagnetic spin correlations along 1D chains as a function of doping. The correlations are quantified by the two-point correlation function

$$C(x) = 4\langle S_i^z S_{i+x}^z \rangle_{\bullet_i \bullet_{i+x}}$$

conditioned on sites i and $i + x$ being singly occupied (filled circles). Experimentally, we prepared Hubbard chains with up to $N = 23$ atoms and post-selected the experimental outcomes to the $S^z = 0$ sector to first consider the effects of doping only. Owing to the underlying harmonic confinement, the atomic cloud is inhomogeneous; using a local density approximation we define the density n as the mean occupation calculated over the sites connecting i to $i + x$ for each value of N (see Methods). From Luttinger liquid theory one expects the wavevector of the SDW to be $k_{\mathrm{SDW}} = 2k_{\mathrm{F}} = \pi n$, where k_{F} is the Fermi wavevector. At finite temperature and large distances $x \gtrsim k_{\mathrm{F}}^{-1}$, the spin correlations are predicted to decay exponentially[1]:

$$C(x) \approx A\mathrm{e}^{-x/\xi}\cos(\pi n x) \qquad (1)$$

where A is a non-universal constant and ξ is the temperature-dependent correlation length that varies[1] weakly with density at $U/t = 7$. We determined A and ξ from an exponential fit of $C(x)$ at half-filling ($n = 1$) for $x = 2, \ldots, 6$, which yields $A = 0.49(4)$ and $\xi = 1.6(1)$ (Fig. 2a), where all distances are expressed in units of the lattice constant d_x (uncertainties denote one standard error of the mean). Away from half-filling, we observe a linear increase of the SDW vector for both hole and charge doping, as revealed by a Fourier transform of the rescaled spin correlation $C(k) = F\{A^{-1}\mathrm{e}^{x/\xi}C(x)\}$ (Fig. 2b). For a quantitative comparison with theory, we show in Fig. 2c the spin correlations $C(x)$ as a function of density n together with QMC calculations for a homogeneous system at temperature $T = 0.29t_x$, as well as the long-distance Luttinger prediction of equation (1). The spin correlations are found to oscillate with a periodicity of $k_{\mathrm{SDW}} = \pi n$, as expected from Luttinger theory. We attribute the microscopic-scale origin of the incommensurate correlations to delocalized doublons and holes, which increase the distance between antiferromagnetically correlated spins[21,22] and thus the wavelength of the SDW. The remaining discrepancies between the experiment, QMC calculations and the Luttinger liquid theory expectations, which are mostly visible at large distances and low densities, are attributed to the trap that induces inhomogeneous density profiles and to averaging over different chain lengths, leading to corrections to the exponential decay.

Incommensurate spin correlations are also expected to appear in the 1D Hubbard model when a spin imbalance is introduced. To isolate the effect of polarization from the influence of doping, we consider the connected two-point spin correlations $C(\tilde{x}) = 4(\langle S_{\tilde{i}}^z S_{\tilde{i}+\tilde{x}}^z \rangle - \langle S_{\tilde{i}}^z \rangle \langle S_{\tilde{i}+\tilde{x}}^z \rangle)$ in squeezed space (the tilde notation refers to quantities in squeezed space), which are obtained by removing holes and doublons from the chain in the post-analysis[22]. In squeezed space[23,24] and for large U/t_x, the system is described by a spin-1/2 antiferromagnetic Heisenberg

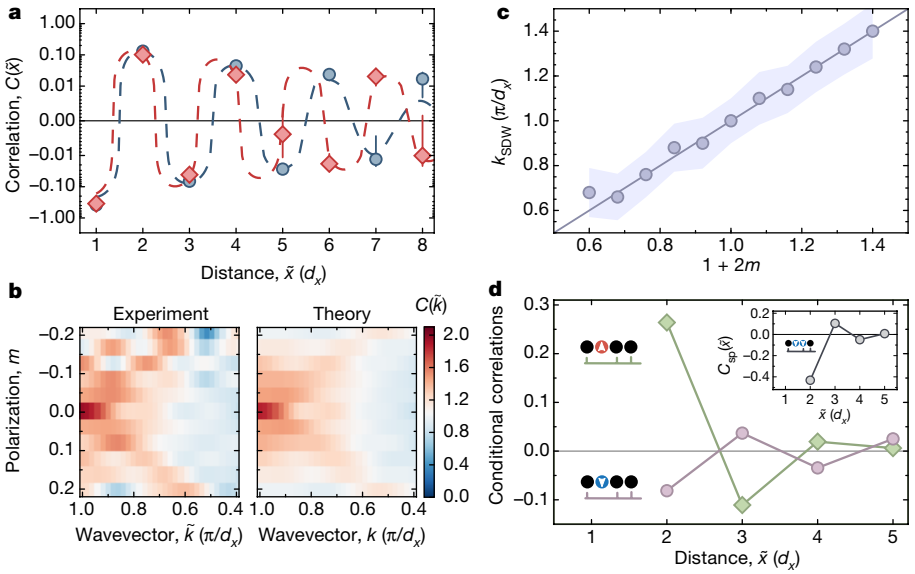

Fig. 3 | Incommensurate spin correlations versus polarization. a, Spin correlations in squeezed space $C(\tilde{x})$ for $m = 0$ (blue) and $m = 0.08$ (red). A sign change is visible at distance $\tilde{x} > 5$, reflecting an increase of the SDW wavelength away from $m = 0$. Dashed lines are fits to the Luttinger liquid theory expectation (equation (2)). **b**, Left, normalized Fourier transform, $C(\tilde{k})$, of $C(\tilde{x})$. The plot exhibits two branches departing from $k = \pi$ when $m \neq 0$, in good agreement with exact diagonalization calculations of the Heisenberg chain at $T = 0.7J$ averaged over the experimental $\{S^z, N_s\}$ (right). The binning of the polarization is in intervals of 0.04. **c**, A linear fit of the branches in **b** yields $k_{SDW} = 1.0(1) \times (1 + 2m)\pi$, in excellent agreement with the Luttinger liquid theory prediction. The shaded region denotes the Fourier-limited systematic error. **d**, Conditional spin correlations across majority $C_{maj}(\tilde{x})$ (violet circles) and minority $C_{min}(\tilde{x})$ (green diamonds) spins for $m = -0.12$. A phase shift of π is visible for the spin correlations across majority spins. Inset, conditional spin correlations across pairs of parallel spins, $C_{sp}(\tilde{x})$, revealing their domain-wall nature in a squeezed space that lies at the origin of the SDW wavelength extension. Error bars denote one standard error of the mean; in **d**, they are smaller than the symbols.

model at a polarization $m = S^z/N_s$, where N_s is the number of singly occupied sites (singlons; see Methods). For the Heisenberg chain, Luttinger liquid theory predicts incommensurate spin correlations that are linear with polarization[1] m at large distances:

$$C(\tilde{x}) \approx A_m e^{-\tilde{x}/\xi_m} \cos[\pi(1+2m)\tilde{x}] \quad (2)$$

where A_m and ξ_m are the polarization- and temperature-dependent amplitude and correlation length, respectively. The SDW wavelength measured by $C(\tilde{x})$ is thus expected to increase away from $m = 0$ because the fixed sampling at the lattice period makes $m > 0$ and $m < 0$ symmetric. Finite-size effects and the dependence[25] of ξ_m on m influence the functional form of the decay (see Methods); therefore we concentrate here on the SDW vector variation predicted by equation (2). In Fig. 3a we show $C(\tilde{x})$ for two polarizations of the chain, $m = 0$ and $m = 0.08$. We observe sign changes in $C(\tilde{x})$ for $\tilde{x} > 5$, which indicate a wavelength extension of the SDW for $m = 0.08$ compared to $m = 0$. To detect the SDW vector variation as a function of polarization without prior assumption of any functional form, we compute the zero-padded Fourier transform of the rescaled spin correlations in squeezed space, $C(\tilde{k}) = F\{C(\tilde{x})/|C(1)|\}$, for each m. It reveals two branches away from $k = \pi$ (see Fig. 3b), for $m > 0$ and $m < 0$, in qualitative agreement with the results of the exact diagonalization of the Heisenberg chain at $T = 0.7J$, where J is the exchange coupling, averaged over our experimental distribution $\{S^z, N_s\}$. In Fig. 3c a linear fit of these branches yields $k_{SDW} = 1.0(1) \times (1 + 2m)\pi$, in remarkable agreement with the Luttinger liquid theory prediction (equation (2)). Similarly to the doped case[21], we now study the microscopic-scale origin of these incommensurate spin correlations. We analyse the spin environment around the majority and minority spins

$$C_{maj}(\tilde{x}) = 4\langle S^z_{\tilde{\imath}} S^z_{\tilde{\imath}+\tilde{x}} \rangle_{S^z \sigma_{\tilde{\imath}+1} > 0}$$
$$C_{min}(\tilde{x}) = 4\langle S^z_{\tilde{\imath}} S^z_{\tilde{\imath}+\tilde{x}} \rangle_{S^z \sigma_{\tilde{\imath}+1} < 0}$$

by measuring the conditional expectation value of the spin correlations in squeezed space for distances $\tilde{x} \geq 2$. The conditioning $S^z \sigma_{\tilde{\imath}+1} > 0$ ($S^z \sigma_{\tilde{\imath}+1} < 0$) means that the spin $\sigma_{\tilde{\imath}+1}$ on site $\tilde{\imath}+1$ is parallel (antiparallel) to the chain magnetization S^z (Fig. 3d). The SDW measured by the correlator $C(\tilde{x})$ is the polarization-dependent weighted average of these two components (see Methods). In Fig. 3d we observe a phase shift of π in the short-distance oscillating part of $C_{maj}(\tilde{x})$, whereas $C_{min}(\tilde{x})$ stays in phase with the unpolarized case. This implies that the excess spins mostly form pairs of parallel majority spins, shifting the antiferromagnetic correlations by one lattice site in the $m \neq 0$ case. In the inset of Fig. 3d we explicitly evaluate the spin correlations across pairs of parallel spins, finding strong antiferromagnetic correlations with opposite parity compared to the unpolarized situation. This demonstrates that excess spins act as domain walls in squeezed space. Similar to the holes in the doped case, the main effect of excess spins is therefore to increase the distance between antiferromagnetically correlated spins, resulting in an increase of the SDW wavelength, as measured by $C(\tilde{x})$. Polarized synthetic Hubbard models have recently been studied also in two dimensions and the emergence of anisotropic spin correlations has been observed[8], but with an unchanged wavevector.

We now explore the evolution of the spin correlations in the 1D–2D crossover, a situation relevant to quasi-1D antiferromagnets[17]. Whereas in 1D there is no magnetic energy cost associated with the delocalization of holes and doublons, this phenomenon is expected to break down in higher dimensions. In a 2D antiferromagnetic background the motion of holes and doublons leads to strings of flipped spins, resulting in the confinement of spin and charge[9,26]. The antiferromagnetic spin correlations around doublons and holes, which are at the origin of the SDW wavelength extension in the doped 1D regime, are therefore expected to qualitatively change in the crossover from one to two dimensions[9]. We prepared 2D clouds with up to 70 atoms and studied spin correlations while varying t_y/t_x between 0 and 1 and keeping $U/t_x = 14$ constant (see Methods). When increasing t_y/t_x, we first observe a decrease in the amplitude of the spin correlations

$$C(x, y) = 4\langle S^z_{i,j} S^z_{i+x,j+y} \rangle_{\bullet_{i,j} \bullet_{i+x,j+y}}$$

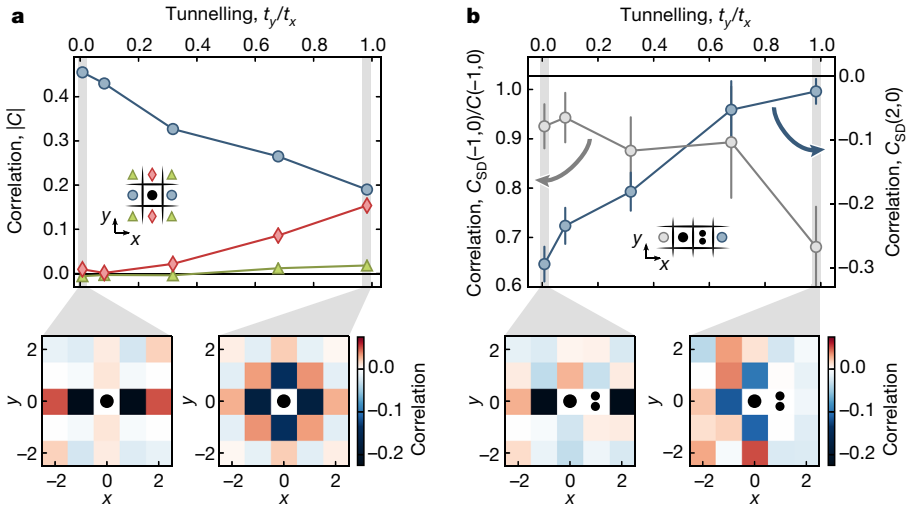

Fig. 4 | Spin correlations in the 1D–2D crossover. a, Spin correlations $C(x, y)$ as a function of the ratio t_y/t_x: $|C(1, 0)|$ (blue circles), $|C(0, 1)|$ (red diamonds) and $|C(1, 1)|$ (green triangles) at $U/t_x = 14$. The spin correlations along x decrease as spin correlations develop in the y direction. The lower panels show the 2D spin correlation amplitudes $C(x, y)$ in the 1D (left) and 2D (right) limits. **b**, Spin correlations across doublons $C_{SD}(2, 0)$ (blue) and next to doublons $C_{SD}(-1, 0)/C(-1, 0)$ (grey) along the x direction. Antiferromagnetic correlations across doublons, at the origin of incommensurate correlations in the 1D limit, are strongly suppressed as spin correlations develop in two dimensions. In this limit the delocalization of doublons also leads to a reduction of antiferromagnetic correlations on neighbouring sites, suggesting the formation of a magnetic polaron. The lower panels show the spin correlations $C_{SD}(x, y)$ between sites (0, 0) (black circle) and (x, y) conditioned on finding a doublon on site (1, 0) (double black circle) in the 1D (left) and 2D (right) case. Error bars in all panels denote one standard error of the mean.

along x and the emergence of spin correlations in the transverse directions (Fig. 4a)[27]. This decrease is expected even at zero temperature and half-filling, where the nearest-neighbour spin correlations $C(1)$ change from -0.6 to -0.36 owing to the higher coordination number modifying the quantum fluctuations[4].

Next, we study the magnetic environment around doublons in the dimensional crossover from one to two dimensions through

$$C_{SD}(x, y) = 4\langle S^z_{i,j} S^z_{i+x,j+y}\rangle_{\bullet_{i,j}\circ_{i+1,j}\bullet_{i+x,j+y}}$$

where the open circle denotes a doublon located at site $(i + 1, j)$ (see Methods). We find that the spin correlations across doublons, $C_{SD}(2, 0)$, are strongly suppressed while 2D spin correlations develop, which is in stark contrast to the 1D case (Fig. 4b). Owing to the harmonic confinement, the few double occupancies are located at the centre of the trap, where the average density is highest and where magnetic correlations are expected to compete with doublon delocalization. In addition to the vanishingly small antiferromagnetic correlations across doublons, we observe a reduction in the nearest-neighbour spin correlations in their vicinity, $C_{SD}(-1, 0)/C(-1, 0)$, to about 70% of the undoped case (Fig. 4b). This suggests the formation of a magnetic polaron[9], which in the extreme limit $U/t \to \infty$ corresponds to the Nagaoka polaron[28]. These local observations provide an initial microscopic-scale picture of the underlying process and explain the recent observation of the global suppression of long-range antiferromagnetic order in two dimensions away from half-filling[29].

Through the direct simultaneous measurement of both density and spin in the doped and spin-imbalanced 1D Hubbard model, we shed light on the connection between incommensurate spin correlations and microscopic-scale degrees of freedom. The spin environment around doublons was found to differ drastically in the 1D and 2D cases, calling for further experimental studies of the formation of magnetic polarons in homogeneous systems[9,30]. Possible routes towards the unambiguous identification of a polaron include the detection of its size using spin correlations and a measurement of its effective mass dynamically or spectroscopically. Another interesting extension of this work is the study of spin correlations as a function of the number of coupled chains, where the parity of the latter is predicted to lead to striking differences between even and odd cases, similarly to the problem of half-integer and integer spin chains[31,32]. At low enough temperature the study of spin and density correlations in hole-doped coupled chains is also expected to reveal a binding of holes to form stripes, which directly extends the domain-wall concept discussed here to two dimensions[33]. A study of such effects through quantum gas microscopy can provide microscopic-scale insights into the physics of the doped repulsive Hubbard model.

Online content

Any methods, additional references, Nature Research reporting summaries, source data, statements of data availability and associated accession codes are available at https://doi.org/10.1038/s41586-018-0778-7.

Received: 23 March 2018; Accepted: 12 October 2018;
Published online 12 December 2018.

1. Giamarchi, T. *Quantum Physics in One Dimension* (Clarendon Press, Oxford, 2003).
2. Greif, D., Uehlinger, T., Jotzu, G., Tarruell, L. & Esslinger, T. Short-range quantum magnetism of ultracold fermions in an optical lattice. *Science* **340**, 1307–1310 (2013).
3. Hart, R. A. et al. Observation of antiferromagnetic correlations in the Hubbard model with ultracold atoms. *Nature* **519**, 211–214 (2015).
4. Parsons, M. F. et al. Site-resolved measurement of the spin-correlation function in the Fermi–Hubbard model. *Science* **353**, 1253–1256 (2016).
5. Boll, M. et al. Spin- and density-resolved microscopy of antiferromagnetic correlations in Fermi–Hubbard chains. *Science* **353**, 1257–1260 (2016).
6. Cheuk, L. W. et al. Observation of spatial charge and spin correlations in the 2D Fermi–Hubbard model. *Science* **353**, 1260–1264 (2016).
7. Drewes, J. H. et al. Antiferromagnetic correlations in two-dimensional fermionic Mott-insulating and metallic phases. *Phys. Rev. Lett.* **118**, 170401 (2017).
8. Brown, P. T. et al. Spin-imbalance in a 2D Fermi–Hubbard system. *Science* **357**, 1385–1388 (2017).
9. Dagotto, E. Correlated electrons in high-temperature superconductors. *Rev. Mod. Phys.* **66**, 763–840 (1994).
10. Haldane, F. D. M. 'Luttinger liquid theory' of one-dimensional quantum fluids. I. Properties of the Luttinger model and their extension to the general 1D interacting spinless Fermi gas. *J. Phys. C Solid State Phys.* **14**, 2585–2609 (1981).
11. Wen, X. G. Chiral Luttinger liquid and the edge excitations in the fractional quantum Hall states. *Phys. Rev. B* **41**, 12838–12844 (1990).
12. Frahm, H. & Korepin, V. E. Correlation functions of the one-dimensional Hubbard model in a magnetic field. *Phys. Rev. B* **43**, 5653–5662 (1991).
13. Cardy, J. *Scaling and Renormalization in Statistical Physics* (Cambridge Univ. Press, Cambridge, 1996).
14. Bockrath, M. et al. Luttinger-liquid behaviour in carbon nanotubes. *Nature* **397**, 598–601 (1999).
15. Lee, J. et al. Real space imaging of one-dimensional standing waves: direct evidence for a Luttinger liquid. *Phys. Rev. Lett.* **93**, 166403 (2004).

16. Stone, M. B. et al. Extended quantum critical phase in a magnetized spin-1/2 antiferromagnetic chain. *Phys. Rev. Lett.* **91**, 037205 (2003).
17. Lake, B., Tennant, D. A., Frost, C. D. & Nagler, S. E. Quantum criticality and universal scaling of a quantum antiferromagnet. *Nat. Mater.* **4**, 329–334 (2005).
18. Klanjšek, M. et al. Controlling Luttinger liquid physics in spin ladders under a magnetic field. *Phys. Rev. Lett.* **101**, 137207 (2008).
19. Tranquada, J. M., Sternlieb, B. J., Axe, J. D., Nakamura, Y. & Uchida, S. Evidence for stripe correlations of spins and holes in copper oxide superconductors. *Nature* **375**, 561–563 (1995).
20. Omran, A. et al. Microscopic observation of Pauli blocking in degenerate fermionic lattice gases. *Phys. Rev. Lett.* **115**, 263001 (2015).
21. Hilker, T. A. et al. Revealing hidden antiferromagnetic correlations in doped Hubbard chains via string correlators. *Science* **357**, 484–487 (2017).
22. Kruis, H. V., McCulloch, I. P., Nussinov, Z. & Zaanen, J. Geometry and the hidden order of Luttinger liquids: the universality of squeezed space. *Phys. Rev. B* **70**, 075109 (2004).
23. Ogata, M. & Shiba, H. Bethe–Ansatz wave function, momentum distribution, and spin correlation in the one-dimensional strongly correlated Hubbard model. *Phys. Rev. B* **41**, 2326–2338 (1990).
24. Woynarovich, F. Excitations with complex wavenumbers in a Hubbard chain. I. States with one pair of complex wavenumbers. *J. Phys. C* **15**, 85–96 (1982).
25. Bogoliubov, N. M., Izergin, A. G. & Korepin, V. E. Critical exponents for integrable models. *Nucl. Phys. B* **275**, 687–705 (1986).
26. Brinkman, W. F. & Rice, T. M. Single-particle excitations in magnetic insulators. *Phys. Rev. B* **2**, 1324–1338 (1970).
27. Greif, D., Jotzu, G., Messer, M., Desbuquois, R. & Esslinger, T. Formation and dynamics of antiferromagnetic correlations in tunable optical lattices. *Phys. Rev. Lett.* **115**, 260401 (2015).
28. White, S. R. & Affleck, I. Density matrix renormalization group analysis of the Nagaoka polaron in the two-dimensional *t*–*J* model. *Phys. Rev. B* **64**, 024411 (2001).
29. Mazurenko, A. et al. A cold-atom Fermi–Hubbard antiferromagnet. *Nature* **545**, 462–466 (2017).
30. Grusdt, F. et al. Parton theory of magnetic polarons: mesonic resonances and signatures in dynamics. *Phys. Rev. X* **8**, 011046 (2017).
31. Dagotto, E. & Rice, T. M. Surprises on the way from one- to two-dimensional quantum magnets: the ladder materials. *Science* **271**, 618–623 (1996).
32. White, S. R. & Scalapino, D. J. Hole and pair structures in the *t*–*J* model. *Phys. Rev. B* **55**, 6504–6517 (1997).
33. White, S. R. & Scalapino, D. J. Density matrix renormalization group study of the striped phase in the 2D *t*–*J* model. *Phys. Rev. Lett.* **80**, 1272–1275 (1998).

Acknowledgements We thank T. Giamarchi for exchanges on incommensurate magnetism, D. Huse, A. Recati, E. Demler and F. Grusdt for discussions and P. Sompet for reading the manuscript. Financial support was provided by the Max Planck Society (MPG) and the European Union (UQUAM, QSIMGAS, MIR-BOSE), and J.K. acknowledges funding from the Hector Fellow Academy.

Reviewer information *Nature* thanks M. Lewenstein, C. de Morais Smith and the other anonymous reviewer(s) for their contribution to the peer review of this work.

Author contributions G.S., T.A.H., J.K., J.V., I.B. and C.G. planned the experiment and analysed and discussed the data. J.N. and L.P. performed the QMC simulations. All authors contributed to the interpretation of the data and the writing of the manuscript.

Competing interests The authors declare no competing interests.

Additional information
Extended data is available for this paper at https://doi.org/10.1038/s41586-018-0778-7.
Reprints and permissions information is available at http://www.nature.com/reprints.
Correspondence and requests for materials should be addressed to G.S.
Publisher's note: Springer Nature remains neutral with regard to jurisdictional claims in published maps and institutional affiliations.

METHODS

Ultracold lattice gas preparation. The experimental protocol used in the experiments reported here closely followed our previous work[21]. Our experiments started with a degenerate spin mixture of ^{6}Li atoms in the lowest two Zeeman states, $|\pm\rangle = |F = 1/2, m_F = \pm 1/2\rangle$ (where F and m_F define the hyperfine state) trapped in a single plane of a vertical optical lattice. The lattice spacing was 3.1 μm and the depth was $17E_r^z$ ($27E_r^z$) in the 1D (crossover) case, where $E_r^i = h^2/(8md_i^2)$ is the recoil energy, m the atomic mass and d_i the lattice spacing along direction i. The total atom number N of the cloud was tuned by varying the depth of a radial trap at the endpoint of the evaporative cooling procedure[20]. To simulate the single-band 1D Hubbard model, we first prepared 1D systems by ramping up the large spacing component ($d_y = 2.3$ μm) of an optical superlattice in the y direction. The lattice was ramped linearly in two steps, first to $15E_r^y$ in 55 ms and then to $27E_r^y$ in 45 ms, which resulted in a final transverse tunnelling of $t_y/h = 1.2$ Hz. With a delay of 10 ms with respect to the start of the y-lattice ramp, the lattice along the tubes (x direction; spacing $d_x = 1.15$ μm) was turned on. The chosen ramp was again composed of two linear parts, the first was a ramp to $3E_r^x$ in 45 ms and the second to $5E_r^x$ in 55 ms. Simultaneously the scattering length was increased from $530a_B$ to $2{,}000a_B$ (where a_B is the Bohr radius) using a magnetic offset field close to the Feshbach resonance, which is located at 834.1 G. At the end of the ramps, the tunnelling along the Hubbard chains reached $t_x/h = 410$ Hz and the on-site interaction $U/h = 2.9$ kHz. The latter was calculated from the ground-band Wannier functions, neglecting higher-band corrections[34]. The corresponding final superexchange coupling was $J_x = 4t_x^2/U = h \times 235$ Hz.

To explore the Hubbard model in the 1D–2D crossover we first ramped up the large spacing component of the superlattice in the y direction to $0.2E_r^y$ in 60 ms and then to depths varying between $5E_r^y$ and $27E_r^y$ in 220 ms. The x-lattice ramp to depths varying between $9E_r^x$ and $10.6E_r^x$ in 280 ms started simultaneously with the second part of the y-lattice ramp. The magnetic offset field was adjusted to maintain a constant ratio of $U/t_x = 14$ at the end of the ramps. A local Stern–Gerlach detection technique[5] with a transverse magnetic field gradient of 95 G cm^{-1} was used to detect both the spin and the density on each lattice site with a fidelity of 97%.

Data analysis. Thanks to our local access to both the spin and the occupation at each lattice site in a single experimental run, we can group each Hubbard chain data by $\{j, N, S^z\}$, where j is the coordinate of the Hubbard chain in the y direction. This allows us to explore different filling and spin sectors (Extended Data Fig. 1). To study the effect of doping on spin correlations we only analysed the data in the $S^z = 0$ sector. The density profile along x is inhomogeneous and dependent on N and j, owing to the underlying harmonic confinement of $\omega = 2\pi \times 200(20)$ Hz. For each pair $\{j, N\}$ we computed a mean density profile $n_j(i, N)$ by averaging the occupation on each site i over different experimental realizations (Extended Data Fig. 2). The reported density, at which spin correlations between sites i and $i + x$ were analysed, is the mean density between the two points $n_j(i, x, N) = (1/x)\sum_{k=i}^{i+x} n_j(k, N)$

To highlight the oscillatory behaviour of the spin correlations as a function of density we considered the two-point spin correlations between sites i and $i+x$, conditioned on having single occupancies (filled circles) on these sites for each pair $\{j, N\}$:

$$C_{i,j,N}(x) = 4\langle S_i^z S_{i+x}^z \rangle_{\bullet_i \bullet_{i+x} j,N} + c(N) \tag{3}$$

where the angle brackets denote averaging over experimental runs, and $c(N)$ is a finite-size offset that depends on the atom number N and the temperature, which we experimentally found to be well described[21] by $c(N) = 1/(N-1) - 0.04(5)$. We also analysed the data in terms of the corresponding connected correlator and found them to agree with the non-connected version in equation (3) within statistical uncertainty. This check was also performed for all other non-connected correlators that we used in this work. Owing to the absence of density–density correlations beyond $x = 1$, this correlation function can be understood as being a renormalized two-point spin correlation[21] $C_{i,j,N}(x) \approx [4\langle S_i^z S_{i+x}^z \rangle_{i,j,N} - c(N)]/n_j(i, x, N)^2$. Finally we grouped all the $C_{i,j,N}(x)$ correlations according to their density $n_j(i, x, N)$ in bins of width $\Delta n = 0.1$ to compute the average spin correlation $C(x)$ for each n shown in Fig. 2.

The microscopic-scale origin of the incommensurate SDW is revealed by the spin correlations across holes and double occupancies shown in Extended Data Fig. 2b:

$$C_{i,y,N}^{\mathrm{dw}}(x) = 4\langle S_i^z S_{i+x}^z \rangle_{\bullet_i \circ_{i+1} \bullet_{i+x} y,N} + c(N)$$

where the open circles denote a doublon or a hole on site $i + 1$. The angle brackets indicate averaging over all experimental realizations in which these conditions are fulfilled. Both the holes and the doublons displace the spin correlations, leading to an increase of their wavelength.

To separate the effect of polarization on the spin correlations from the charge sector, we studied spin correlations in squeezed space. Here, we extend the concept of squeezed space to finite U by removing doublons and holes only when these are not nearest neighbours. The latter condition is supported by the strong doublon–hole bunching at $|x| = 1$, measured by $g_2(x) = -1 + \langle d_0 h_x \rangle / (\langle d_0 \rangle \langle h_x \rangle)$, where d_i and h_j denote the doublon and hole operators on sites i and j, respectively (see Extended Data Fig. 3a), which we attribute to quantum fluctuations. The full dataset in this measurement consisted of 26,442 Hubbard chains, which we prepared close to half-filling at the centre of the trap. This led to shorter chains with up to $N = 16$ atoms. We decided to use the squeezed space analysis instead of post-selecting the data to the zero-hole and -doublon sector to improve our statistics. Within statistical uncertainties, the post-selected data are consistent with these squeezed-state results.

The connected spin correlations in squeezed space, indicated by $\tilde{\imath}$ and $\tilde{x}$, are defined as

$$C_{\tilde{\imath},j,N_s,S^z}(\tilde{x}) = 4(\langle S_{\tilde{\imath}}^z S_{\tilde{\imath}+\tilde{x}}^z \rangle - \langle S_{\tilde{\imath}}^z \rangle \langle S_{\tilde{\imath}+\tilde{x}}^z \rangle) + c_{\mathrm{sq}}(N_s)$$

where the number of singly occupied sites N_s includes nearest-neighbour doublon–hole pairs. We again take into account a finite-size offset $c_{\mathrm{sq}}(N_s)$ similar[21] to $c(N)$, which we obtain by taking the mean of the correlator at distances $\tilde{x} = 4, \ldots, 7$. The magnetization of the effective Heisenberg chain in squeezed space is defined as $m = S^z/N_s$. We group all the $C_{\tilde{\imath},j,N_s,S^z}(\tilde{x})$ correlations by their polarization m in bins of width $\Delta m = 0.04$ to compute the average spin correlation C shown in Fig. 3. The Fourier transform shown in Fig. 3b is calculated using our experimental points $\tilde{x} = 1, \ldots, 10$, which limits our $\tilde{k}$-space resolution, and is zero-padded to increase the visibility of the SDW vector change.We highlight in Extended Data Fig. 4 the quantitative agreement in the fixed-distance comparison of $C(\tilde{x})$ with exact diagonalization results of the Heisenberg chain at $T = 0.7J$ averaged over our experimental $\{S^z, N_s\}$ distribution. This validates the use of the squeezed-space concept away from $S^z = 0$. Similarly to the doped case, the microscopic-scale origin of the polarization dependence of the SDW wavelength can be explained in terms of domain walls in squeezed space. From the sum rule for conditional probabilities we can write

$$\begin{aligned} C(\tilde{x}) = \Big(& 4\langle S_{\tilde{\imath}}^z S_{\tilde{\imath}+\tilde{x}}^z \rangle_{S^z \sigma_{\tilde{\imath}+1} > 0} \times p_{S^z \sigma_{\tilde{\imath}+1} > 0} \\ & + 4\langle S_{\tilde{\imath}}^z S_{\tilde{\imath}+\tilde{x}}^z \rangle_{S^z \sigma_{\tilde{\imath}+1} < 0} \times p_{S^z \sigma_{\tilde{\imath}+1} < 0} \Big) \\ & - 4\langle S_{\tilde{\imath}}^z \rangle \langle S_{\tilde{\imath}+\tilde{x}}^z \rangle \end{aligned} \tag{4}$$

where $\langle X \rangle_Y$ denotes the conditional expectation value of X given Y, and p_Y is the probability of event Y. Intuitively, for low enough polarization, the spin correlations at short distances around the minority spins will remain in phase with the unpolarized case on average to minimize the magnetic energy. The short-distance spin correlations around the majority spins, on the other hand, are expected to be more sensitive to polarization. We consider the oscillating part of the two conditional expectations in the parentheses in equation (4) for $m = -0.12$ in Fig. 3d after removing a finite-size and polarization-dependent offset similar to $c_{\mathrm{sq}}(N_s)$. We indeed find for $\tilde{x} \leq 5$ antiferromagnetic correlations in phase with the unpolarized case across the minority spins, whereas these are phase shifted by π around the majority spins. The sign change of the spin correlations across the majority spins reveals that the polarization is mostly carried by pairs of parallel majority spins, which we find to be delocalized over the full chain. We directly detected pairs of parallel spins, computed the spin correlations across them (inset of Fig. 3d) and found that they indeed act as delocalized domain walls in the antiferromagnet. These domain walls stretch spin correlations and lead to incommensurate magnetism when $m \neq 0$. Examples of domain-wall distributions are shown in Extended Data Fig. 5.

In the dimensional crossover and 2D regime we prepared anisotropic samples consisting of about five coupled Hubbard chains (Extended Data Fig. 6). Similarly to the 1D case, the spin correlations were calculated on singly occupied sites through

$$C_{\boldsymbol{n}}(\boldsymbol{r}) = 4\langle S_{\boldsymbol{n}}^z S_{\boldsymbol{n}+\boldsymbol{r}}^z \rangle_{\bullet_{\boldsymbol{n}} \bullet_{\boldsymbol{n}+\boldsymbol{r}}}$$

averaged over all sites $\boldsymbol{n} = (n_x, n_y)$ where n_i are integers labelling lattice sites. When studying spin correlations around double occupancies and holes at the crossover, we minimized biasing of the correlator by a possibly distorted magnetic background around quantum-fluctuation-induced doublon–hole pairs. The strong bunching observed in the doublon–hole correlations $g_2(\boldsymbol{r})$ (see Extended Data Fig. 6) at the nearest-neighbour scale identifies a strong contribution of quantum fluctuations to these correlations. Hence, we discarded any doublons with one unoccupied nearest neighbour from the analysis of the spin correlations.

Quantum Monte Carlo calculations. The QMC results reported here were obtained in a similar fashion as those found in ref. [5]. Simulating the fermionic system was possible by mapping between the 1D fermionic Hubbard model and a system of two hard-core bosonic species with on-site interspecies interactions[35].

We used the worm algorithm[36] in the implementation of ref. [37]. This algorithm exhibits a linear scaling in the system volume when simulating the resulting bosonic model. The spin S_i at site i of the fermionic model is mapped onto a diagonal observable with respect to the Fock basis $\{|\ldots, n_j, \ldots\rangle\}$ of the bosonic model, which is proportional to the differences in the occupation numbers of the bosonic particles at the same site.

The simulations were all carried out in the grand canonical ensemble. The system consisted of a homogeneous lattice of $L = 20$ sites with hard-wall boundary conditions. This size was confirmed to be large enough to avoid finite-size corrections. We note however that the correlations were affected by an unavoidable systematic offset that scales as $1/N$, which was corrected for in the analysis, as explained above.

To better mimic the measurement procedure of the actual experiment, we saved the raw QMC configurations and performed the analysis off-line. In this process, care must be taken to make sure that subsequent configurations are decorrelated. A further blocking and jackknife estimation was used to rule out any residual correlation.

The off-line analyses were subject to the same filtering procedures for the occupation and magnetization sector as in the experimental procedure. To gather enough statistics for the different values of the density that were accessible in the experiment, we tuned the chemical potentials of the two bosonic species so as to have symmetric mixtures with total density n between 0.4 and 1.2.

Data availability

The datasets generated and analysed during this study are available from the corresponding author upon reasonable request.

34. Büchler, H. P. Microscopic derivation of Hubbard parameters for cold atomic gases. *Phys. Rev. Lett.* **104**, 090402 (2010).
35. Jordan, P. & Wigner, E. Über das Paulische Äquivalenzverbot. *Z. Phys.* **47**, 631–651 (1928).
36. Prokof'ev, N. V., Svistunov, B. V. & Tupitsyn, I. S. Exact, complete, and universal continuous-time worldline Monte Carlo approach to the statistics of discrete quantum systems. *J. Exp. Theor. Phys.* **87**, 310–321 (1998).
37. Pollet, L., Houcke, K. V. & Rombouts, S. M. Engineering local optimality in quantum Monte Carlo algorithms. *J. Comput. Phys.* **225**, 2249–2266 (2007).

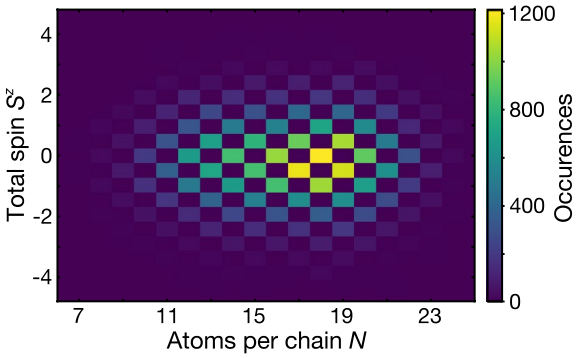

Extended Data Fig. 1 | Chain statistics. Hubbard chain statistics are shown for a typical dataset containing 5,240 shots. The total spin S^z and total atom number N of individual Hubbard chains are conserved quantities of the Hamiltonian for each experimental run. However, they fluctuate for different experimental realizations, allowing us to explore the effects of doping and polarization individually through data grouping.

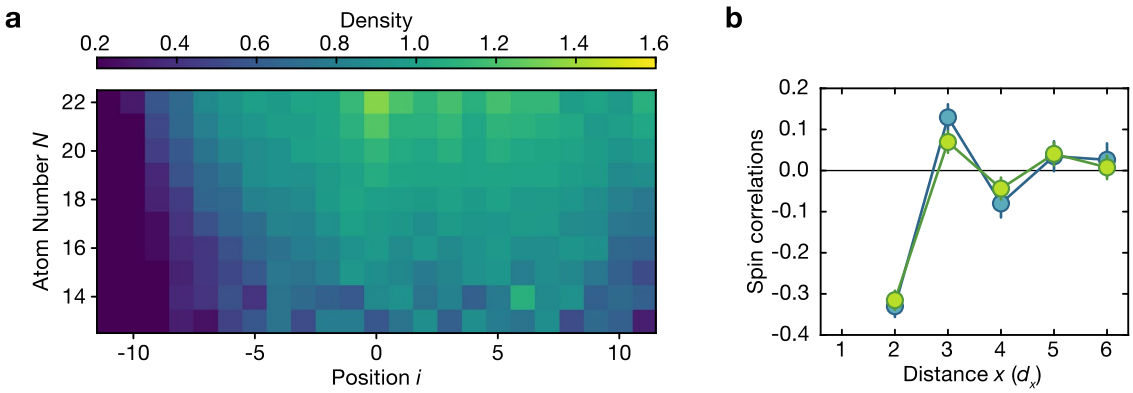

Extended Data Fig. 2 | Density properties of the 1D clouds. a, Density profiles $n_0(i, N)$ of the chain located at the centre of the cloud in the y direction ($j = 0$). **b**, Antiferromagnetic spin correlations across a hole fixed at $x = 1$ (green) or a doublon (blue), measured through $C^{dw}(x)$. The correlation signal is shifted by the hole, which is the microscopic-scale origin of the incommensurate spin correlations away from half-filling in the spin-balanced case. Error bars denote one standard error of the mean.

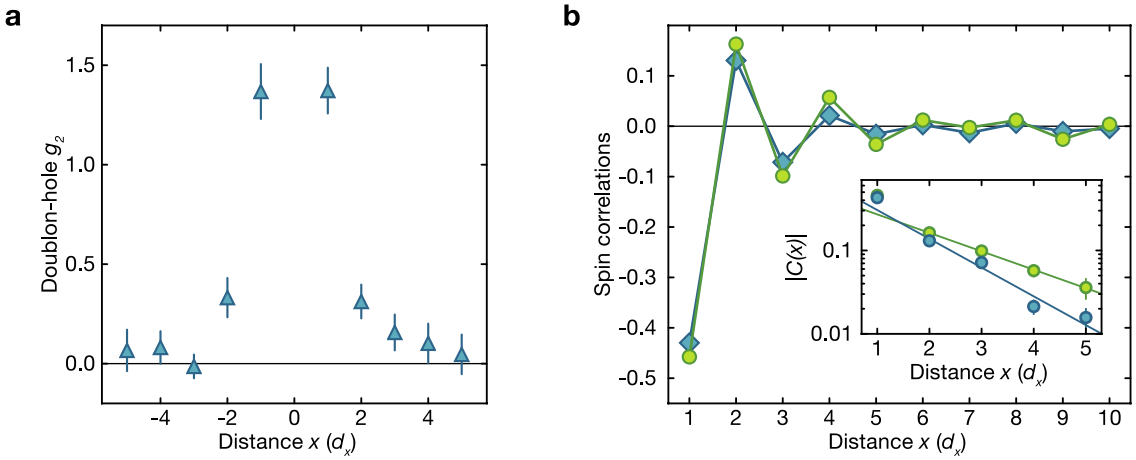

Extended Data Fig. 3 | Spin correlations in squeezed space. a, Doublon–hole correlations, measured by $g_2(x)$. The strong bunching at $|x| = 1$ reveals neighbouring doublon–hole pairs as mostly stemming from quantum fluctuations. This justifies our extension of the squeezed-space concept away from $U \to \infty$. **b**, Spin correlations in the zero-magnetization sector at the centre of the cloud. Averaging over different polarizations (blue) results in a faster decay of the spin correlations with distance x in squeezed space compared to the $S^z = 0$ sector (green). Exponential fits of the correlation envelope for distances $x = 2, \ldots, 6$ yield $\xi_{\mathrm{avg}} = 1.3(1)$ without magnetization post-selection and $\xi_0 = 2(1)$ in the $S^z = 0$ sector. Error bars denote one standard error of the mean.

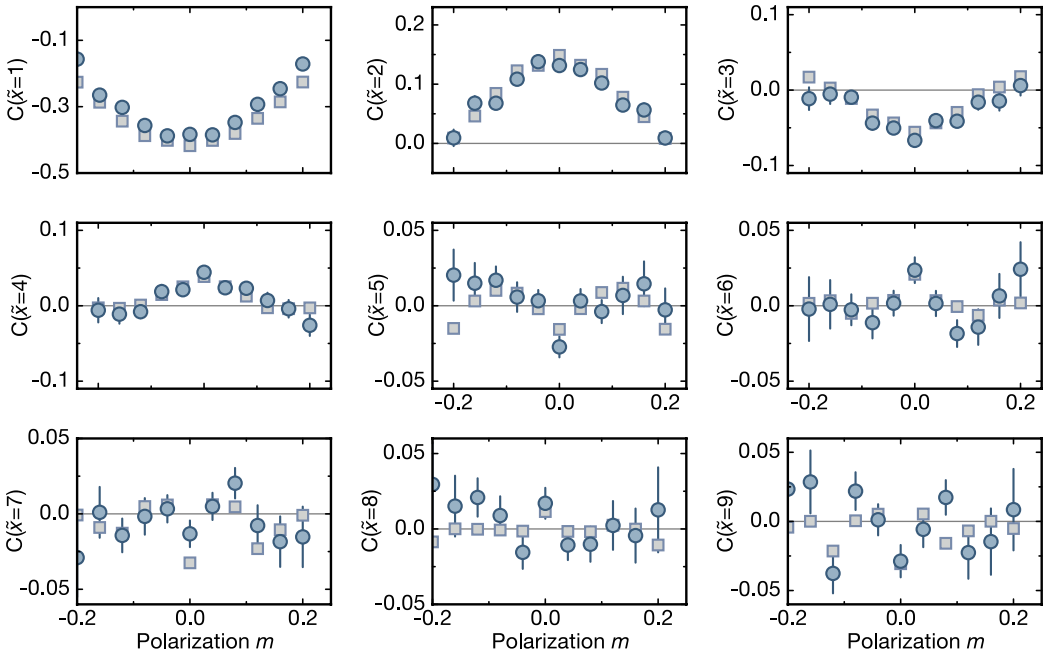

Extended Data Fig. 4 | Squeezed-space spin correlations at fixed distance. Experimental spin correlations in squeezed space are shown as a function of polarization m for distances $\tilde{x} = 1, \ldots, 9$ (blue circles), along with exact diagonalization results for spin correlations in the Heisenberg chain at $T = 0.7J$ averaged over the experimental $\{S^z, N_s\}$ distribution (grey squares). Error bars denote one standard error of the mean.

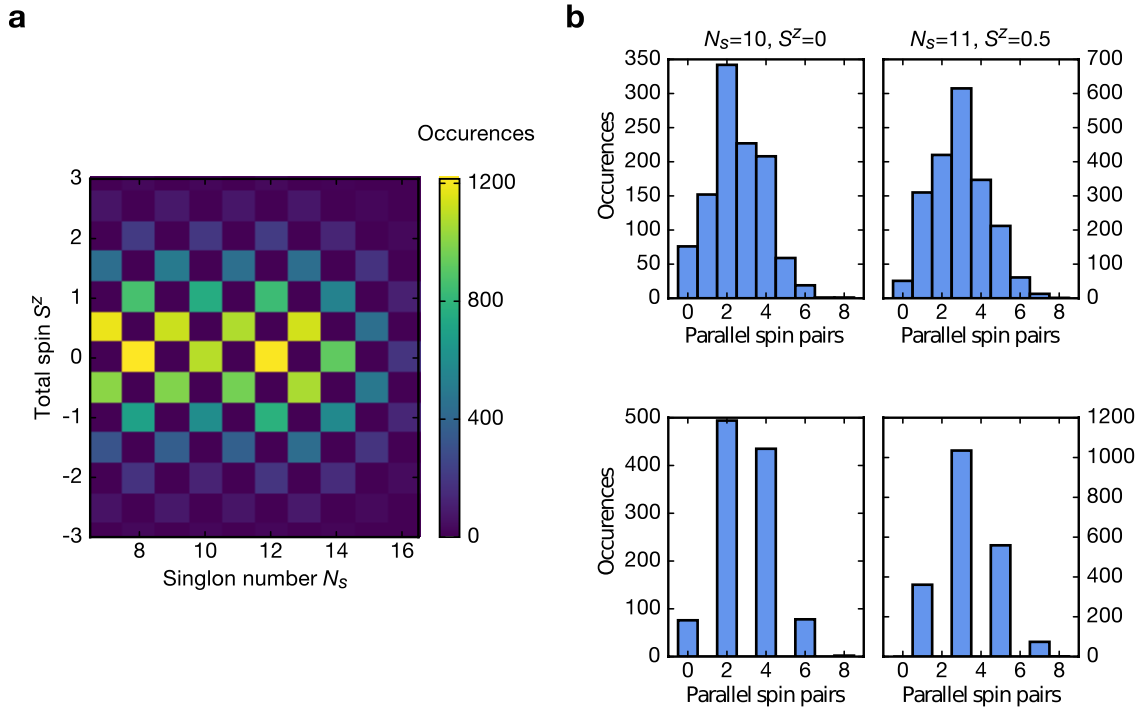

Extended Data Fig. 5 | Chain statistics for the polarization study. **a**, Experimental distribution $\{S^z, N_s\}$ used for studying the effects of polarization on the SDW vector. **b**, Histograms of pairs of parallel spins for $\{N_s = 10, S^z = 0\}$ and $\{N_s = 11, |S^z| = 0.5\}$. The upper row shows, as expected, an upward shift of the distribution towards larger number of domain walls away from $S^z = 0$. By using the convention that spins pointing in the same direction at the edges contribute as one pair of parallel spins (lower row), we find that the parity of the number of domain walls is even in the integer-spin sectors and odd in the half-integer case. In the $S^z = 0$ sector, domain walls appear in pairs of opposite quantum numbers, which do not affect the SDW wavevector. In the $|S^z| = 0.5$ case on the other hand, we find a minimum of one domain wall owing to the excess spin and higher numbers of domain walls corresponding to pairs of additional excited parallel-spin pairs with opposite quantum numbers.

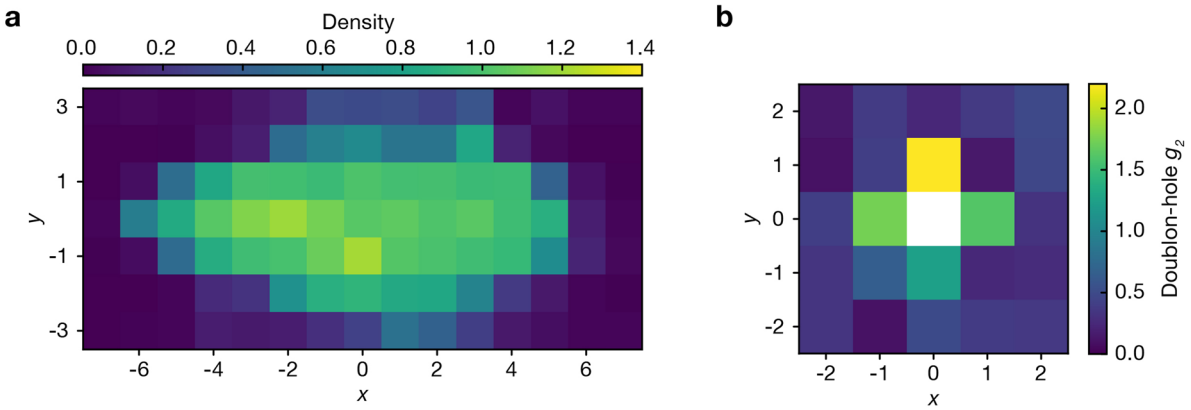

Extended Data Fig. 6 | Properties of the prepared 2D clouds. a, Density distribution for $t_y/t_x = 1$. **b**, Doublon–hole correlations $g_2(\boldsymbol{r})$. The strong bunching of the doubon–hole correlations $g_2(\boldsymbol{r})$ at $|\boldsymbol{r}| = 1$ justifies the rejection of outcomes in which holes and doublons are found nearby when studying the effects of doping.